Indonesian Journal of Aerospace Vol. 22 No. 2 Desember 2024 : pp 151 – 166 (Andria et al.)
DOI: 10.59981/ijoa.2024.8949
https://ejournal.brin.go.id/ijoa/

A Corotational Formulation For Geometrically Nonlinear Dynamics of 2D Flexible Beams

Novi Andria[1], Lavi Rizki Zuhal[2], Hari Muhammad[2], Leonardo Gunawan[2]

[1]Rocket Technology Center, National Research and Innovation Agency – BRIN, Bogor, Jawa Barat, 16350, Indonesia
[2]Department of Aeronautics and Astronautics, Faculty of Mechanical and Aerospace Engineering, Institut Teknologi Bandung, Jl. Ganesha 10, Bandung, Jawa Barat, 40132, Indonesia
e-mail: novi020@brin.go.id

Received: 30-11-2024. Accepted: 16-12-2024. Published: 20-05-2025

Abstract

A simple and efficient 2D corotational formulation for dynamic analysis of geometrically nonlinear flexible beams is presented in this paper. The corotational approach can easily facilitate the evaluation of internal elastic forces by introducing an element frame to separate rigid body motion and the deformational part. In the present study, the Euler-Bernoulli beam model with a simple geometric stiffness matrix is employed and Newmark's implicit time-stepping scheme with an iterative predictor-corrector algorithm is adopted. The validity and efficiency of the present corotational formulation are verified by simulating three numerical examples. Despite its simple numerical implementation, simulation results confirm that the proposed formulation is highly accurate and efficient in simulating flexible beams undergoing large deformation.

Keywords: *2D corotational formulation, geometrically nonlinear, flexible beam, dynamic analysis.*

Nomenclature

$\mathbf{q}$	=	displacement vector in the global coordinate system
$\bar{\mathbf{q}}$	=	displacement vector in the local coordinate system
$\mathbf{q}^r$	=	rigid body displacement vector
$\hat{\mathbf{q}}$	=	element deformation vector
u	=	axial displacement
w	=	transversal displacement
θ	=	rotation, degree
α	=	inclination angle from the initial configuration to the current configuration
l	=	element length
β	=	the current angle of the local coordinate system with respect to the global coordinate system
β_0	=	inclination of the initial frame measured counterclockwise from the global X-axis to the local x-axis
$\mathbf{T}$	=	transformation matrix
$\mathbf{N}$	=	shape function
Π	=	strain energy
$\mathbf{k}$	=	element stiffness matrix in the local coordinate system
$\mathbf{K}$	=	element stiffness matrix in the global coordinate system

A = cross-sectional area
KE = kinetic energy
$\mathbf{m}$ = element mass matrix in the local coordinate system
$\mathbf{M}$ = element mass matrix in the global coordinate system
$\mathbf{C}$ = element damping matrix in the global coordinate system
$\mathbf{F}^{\text{int}}$ = internal load vector
$\mathbf{F}^{\text{ext}}$ = external load vector
$\dot{\mathbf{q}}$ = velocity vector
$\ddot{\mathbf{q}}$ = acceleration vector
$\mathbf{R}$ = residual load
Φ = residual energy
$\mathrm{d}\mathbf{q}$ = residual displacement
n = time step
L = length
b = width
h = thickness
I = area moment of inertia
E = Young's modulus
v = Poisson's ratio
ρ = material density
dt = time step size

1. Introduction

Flexible beams are frequently encountered in many engineering applications, for instance, in aircraft structures, multi-stage rockets, and submarine pipelines. Large deformation with small strain can be experienced by these structures. Linear approach is not sufficient to perform structural analysis for these structures since large deformation yields geometric nonlinearity. This geometrically nonlinear behavior is usually simulated using nonlinear finite element method, generally based on Total Lagrangian Formulation (TLF) and Updated Lagrangian Formulation (Kan et al., 2021). However, the conventional FEM remains to have some drawbacks when dealing with geometrically nonlinear problems due to the existence of mesh distortion when the structures undergo large deformation (Durand et al., 2019; Wang et al., 2013).

Corotational formulation is another approach to addressing geometrically nonlinear problems (Le et al., 2011, 2012, 2014a, 2014b; Kan et al., 2021; Ma et al., 2023; You et al., 2024). In corotational formulation, the motion of the structural element is decomposed into rigid body motion and the deformational parts. A local coordinate system, attached rigidly to the element, translates and rotates with the element during the rigid body motion. This local co-rotating coordinate system becomes the reference configuration in calculating element deformation (Le et al., 2014a), implying that linear strain-displacement relation can be applied locally (Levyakov, 2015). Thus, the structure can be efficiently modeled since it allows to reuse of existing linear finite element codes.

The corotational formulation for geometrically nonlinear beams has been developed and implemented by many authors, for instance, see (Alsafadie et al., 2011; Le et al., 2011, 2012, 2014a, 2014b; Kan et al., 2021; Ma et al., 2023; You et al., 2024). For 2D structural analysis, Le et al. (2011, 2012) developed a corotational formulation using Interdependent Interpolation Element (IIE) in combination with shallow arch beam theory. Their formulation was adopted by the author of the present paper to simulate two-dimensional (2D) nonlinear static analysis of large deformation structures (Andria et al., 2019). Elkaranshawy et al. (2018) also devel-

oped a 2D corotational beam formulation by implementing the arc-length integral formula in their internal elastic force calculation to simulate some 2D nonlinear static and dynamics cases.

The current study extends the previous 2D corotational static formulation presented in (Andria et al., 2019) by including dynamic analysis. Local beam element formulation employs the classical Hermitian shape functions. Euler-Bernoulli beam assumption is adopted and the element mass and stiffness matrices are taken from Elkaranshawy et al. (2018). Differing from their corotational formulation, however, the present study does not apply the arc length integration formula to simplify the computation of axial strain. In addition, by assuming a small local rotation, the geometric stiffness matrix of the present formulation is also different from that in (Elkaranshawy et al., 2018). Newmark's implicit method with the predictor-corrector is used as the time-integration scheme. This time-stepping procedure is applied since it assures the best possible stability and convergence (Chróścielewski et al., 2000). The energy-convergent criterion is used to define the dynamic equilibrium of the system. Three numerical examples are presented and compared with existing data from the literature to verify the performance of the present corotational formulation.

2. Methodology

The aim of the current study is to present a simple and efficient 2D corotational algorithm for dynamic analysis of the geometrically nonlinear beam. To illustrate the simplicity of the proposed algorithm, this section briefly presents the kinematics of a 2D beam, followed by an overview of the strain and kinetic energy along with the stiffness and mass matrices and the internal load vectors of the beam. The dynamic equilibrium equation and the time-stepping scheme of the present corotational formulation are given at the end of the section.

2.1. Beam Kinematics

The kinematics of a 2-node beam element is illustrated in Figure 2-1.

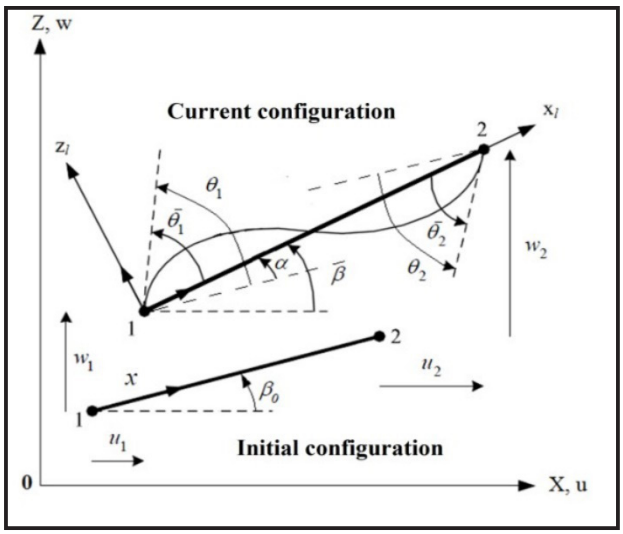

Figure 2-1: Kinematics of a beam element (Le et al., 2011).

The global coordinates (X,Z) for nodes 1 and 2 of the i^{th} beam element are (X_1,Z_1) and (X_2,Z_2), respectively. The global displacement vector is given by:

$$\mathbf{q}_i = [u_1 \quad w_1 \quad \theta_1 \quad u_2 \quad w_2 \quad \theta_2]^T \tag{2-1}$$

while the local displacements vector is defined as:

$$\bar{\mathbf{q}}_i = [\bar{u}_1 \quad \bar{w}_1 \quad \bar{\theta}_1 \quad \bar{u}_2 \quad \bar{w}_2 \quad \bar{\theta}_2]^T \tag{2-2}$$

where

$$\bar{u}_1 = \bar{w}_1 = \bar{w}_2 = 0 \tag{2-3}$$

$$\bar{u}_2 = \bar{u} = (l_n^2 - l_0^2)/(l_n + l_0) \tag{2-4}$$

$$\bar{\theta}_1 = \theta_1 - \alpha = \theta_1 - \beta + \beta_0 \quad (2\text{-}5)$$

$$\bar{\theta}_2 = \theta_2 - \alpha = \theta_2 - \beta + \beta_0 \quad (2\text{-}6)$$

In the current work, instead of implementing the arc-length integral formula as in (Elkaranshawy et al., 2018), a simple calculation as indicated in equation (2-4) is used to calculate the elongation of the beam element. l_0 and l_n in equation (2-4) are the initial and current length of the beam element, respectively, which are defined as:

$$l_n = [(X_2 - X_1)^2 + (Z_2 - Z_1)^2]^{1/2} \quad (2\text{-}7)$$

$$l_0 = [(X_2 + u_2 - X_1 - u_1)^2 + (Z_2 + w_2 - Z_1 - w_1)^2]^{1/2} \quad (2\text{-}8)$$

Equations (2-5) and (2-6) are obtained by adopting Kirchhoff Theory which the normal vector of the beam cross-section is always parallel to the centerline of the beam. β is the current angle of the local coordinate system, which is defined by:

$$c = cos\,\beta = (X_2 + u_2 - X_1 - u_1)/l_n \quad (2\text{-}9)$$

$$s = sin\,\beta = (Z_2 + w_2 - Z_1 - w_1)/l_n \quad (2\text{-}10)$$

Thus,

$$\beta = \text{atan}(s/c) \quad (2\text{-}11)$$

The displacement vectors $\mathbf{q_i}$, $\bar{\mathbf{q}}_\mathbf{i}$ and the rigid body displacement vector $\mathbf{q_i}^r$ are related by:

$$\mathbf{q_i} = \mathbf{q_i}^r + \mathbf{T_i}\bar{\mathbf{q}}_\mathbf{i} \quad (2\text{-}12)$$

Here, $\mathbf{T_i}$ is the i^{th} beam element transformation matrix.

Following Elkaranshawy et al. (2018), the Hermitian shape functions are adopted to relate the element deformation vector $\hat{\mathbf{q}}_\mathbf{i}$ to the element nodal displacement vector $\bar{\mathbf{q}}_\mathbf{i}$, given as follows:

$$\hat{\mathbf{q}}_\mathbf{i} = \mathbf{N_i}\bar{\mathbf{q}}_\mathbf{i} \quad (2\text{-}13)$$

or

$$\begin{pmatrix} \hat{u} \\ \hat{w} \\ \hat{\theta} \end{pmatrix} = \begin{bmatrix} N^1 & 0 & 0 & N^4 & 0 & 0 \\ 0 & N^2 & N^3 & 0 & N^5 & N^6 \\ 0 & N^2 & N^3 & 0 & N^5 & N^6 \end{bmatrix} \bar{\mathbf{q}}_\mathbf{i} \quad (2\text{-}14)$$

where

$$N^1 = 1 - \zeta$$
$$N^2 = 1 - 3\zeta^2 + 2\zeta^3$$
$$N^3 = x(1 - \zeta)^2$$
$$N^4 = \zeta$$
$$N^5 = 3\zeta^2 - 2\zeta^3$$
$$N^6 = x(-\zeta + \zeta^2)$$
$$\zeta = \frac{\mathrm{x}}{l_0} \quad (2\text{-}15)$$

2.2. Strain energy, stiffness matrices, and internal elastic load vectors

The strain energy of the i^{th} beam element can be expressed as:

$$\Pi_\mathrm{i} = \frac{1}{2}\bar{\mathbf{q}}_\mathbf{i}^{\mathrm{T}}\mathbf{k_i}\bar{\mathbf{q}}_\mathbf{i} \quad (2\text{-}16)$$

where $\mathbf{k_i}$ is the element stiffness matrix in the local coordinate system. This matrix can be decomposed into material stiffness matrix ($\mathbf{k_1}$) and geometric stiffness matrix ($\mathbf{k_2}$):

$$\mathbf{k_i} = \mathbf{k_1} + \mathbf{k_2} \quad (2\text{-}17)$$

By assuming small strain ($l_n = l_0$), the forms for the Euler-Bernoulli beam models of these stiffness matrices are given as follows:

$$\mathbf{k}_1 = \frac{E}{l_0}\begin{bmatrix} A_i & 0 & 0 & -A_i & 0 & 0 \\ 0 & \frac{12I_i}{l_0^2} & \frac{6I_i}{l_0} & 0 & -\frac{12I_i}{l_0^2} & \frac{6I_i}{l_0} \\ 0 & \frac{6I_i}{l_0} & 4I_i & 0 & -\frac{6I_i}{l_0} & 2I_i \\ -A_i & 0 & 0 & A_i & 0 & 0 \\ 0 & -\frac{12I_i}{l_0^2} & -\frac{6I_i}{l_0} & 0 & \frac{12I_i}{l_0^2} & -\frac{6I_i}{l_0} \\ 0 & \frac{6I_i}{l_0} & 2I_i & 0 & -\frac{6I_i}{l_0} & 4I_i \end{bmatrix} \tag{2-18}$$

$$\mathbf{k}_2 = EA_i\begin{bmatrix} 0 & -\frac{\bar{\theta}_2+\bar{\theta}_1}{10l_0} & \frac{\bar{\theta}_2-4\bar{\theta}_1}{30} & 0 & \frac{\bar{\theta}_2+\bar{\theta}_1}{10l_0} & -\frac{\overline{4\theta}_2-\bar{\theta}_1}{30} \\ -\frac{\bar{\theta}_2+\bar{\theta}_1}{10l_0} & \frac{36\bar{u}}{30l_0^2} & \frac{\bar{u}}{10l_0} & \frac{\bar{\theta}_2+\bar{\theta}_1}{10l_0} & -\frac{36\bar{u}}{30l_0^2} & \frac{\bar{u}}{10l_0} \\ \frac{\bar{\theta}_2-4\bar{\theta}_1}{30} & \frac{\bar{u}}{10l_0} & \frac{2\bar{u}}{15} & -\frac{\bar{\theta}_2-4\bar{\theta}_1}{30} & -\frac{\bar{u}}{10l_0} & -\frac{\bar{u}}{30} \\ 0 & \frac{\bar{\theta}_2+\bar{\theta}_1}{10l_0} & -\frac{\bar{\theta}_2-4\bar{\theta}_1}{30} & 0 & -\frac{\bar{\theta}_2+\bar{\theta}_1}{10l_0} & \frac{\overline{4\theta}_2-\bar{\theta}_1}{30} \\ \frac{\bar{\theta}_2+\bar{\theta}_1}{10l_0} & -\frac{36\bar{u}}{30l_0^2} & -\frac{\bar{u}}{10l_0} & -\frac{\bar{\theta}_2+\bar{\theta}_1}{10l_0} & \frac{36\bar{u}}{30l_0^2} & -\frac{\bar{u}}{10l_0} \\ -\frac{\overline{4\theta}_2-\bar{\theta}_1}{30} & \frac{\bar{u}}{10l_0} & -\frac{\bar{u}}{30} & \frac{\overline{4\theta}_2-\bar{\theta}_1}{30} & -\frac{\bar{u}}{10l_0} & \frac{2\bar{u}}{15} \end{bmatrix} \tag{2-19}$$

The $\mathbf{k}_2\mathbf{k}_2$ stiffness matrix in equations (2-17) and (2-19) is the nonlinear term generated when the beam undergoes large deformation. By further assuming small local rotation ($\bar{\theta}_1 = \bar{\theta}_2 \approx 0\bar{\theta}_1 = \bar{\theta}_2 \approx 0$), the geometric stiffness matrix in eq. (2-19) becomes:

$$\mathbf{k}_2 = f_{x_2}\begin{bmatrix} 0 & 0 & 0 & 0 & 0 & 0 \\ 0 & 36 & 3l_0 & 0 & -36 & 3l_0 \\ 0 & 3l_0 & 4l_0^2 & 0 & -3l_0 & -l_0^2 \\ 0 & 0 & 0 & 0 & 0 & 0 \\ 0 & -36 & -3l_0 & 0 & 36 & -3l_0 \\ 0 & 3l_0 & -l_0^2 & 0 & -3l_0 & 4l_0^2 \end{bmatrix} \tag{2-20}$$

where

$$f_{x_2} = \frac{EA_i\bar{u}}{30l_0^2} \tag{2-21}$$

This $\mathbf{k}_2$ matrix is different from that in (Elkaranshawy et al., 2018) in terms of the value of f_{x_2} in which they wrote it as $f_{x_2} = \frac{EA_i\bar{u}}{30}$.

It can be clearly seen that the $\mathbf{k}_2$ stiffness matrix in eq. (2-20) does not have any time-dependent terms. Thus this geometric stiffness matrix can be evaluated once and stored at the beginning of the simulation. The fact that this matrix is not computed at every time step, together with the use of simple computation of axial strain, will obviously enhance the computational efficiency of the proposed corotational formulation. However, it should be noted that the small local rotation assumption is only applied for the derivation of the geometric stiffness matrix.

In the global coordinate system, the element stiffness matrix $\mathbf{K_i}$ can be defined as follows:

$$\mathbf{K_i} = \mathbf{T_i}\mathbf{k_i}\mathbf{T_i}^{\mathrm{T}} \tag{2-22}$$

The internal elastic load vector ($\mathbf{F_i^{int}}$) in the global coordinate system can be formulated as follows:

$$\mathbf{F_i^{int}} = \mathbf{T_i}\mathbf{f_i^{int}} \tag{2-23}$$

where $\mathbf{f_i^{int}}$ is the internal elastic load vector in the local coordinate system, defined as:

$$\mathbf{f}_i^{int} = \mathbf{k}_i \bar{\mathbf{q}}_i \tag{2-24}$$

2.3. Kinetic energy and mass matrices

The kinetic energy of the ith beam element takes form:

$$KE_i = \frac{1}{2} \dot{\mathbf{q}}_i{}^T \mathbf{M}_i \dot{\mathbf{q}}_i \tag{2-25}$$

where $\dot{\mathbf{q}}_i$ is the nodal velocity vector of the ith beam element in the global coordinate system and $\mathbf{M}_i$ is the element mass matrix in the global coordinate system, which defined as:

$$\mathbf{M}_i = \mathbf{T}_i \mathbf{m}_i \mathbf{T}_i{}^T \tag{2-26}$$

The element mass matrix ($\mathbf{m}_i$) in equation (2-25) can be written as:

$$\mathbf{m}_i = \mathbf{m}_1 + \mathbf{m}_2 \tag{2-27}$$

The forms $\mathbf{m}_1$ and $\mathbf{m}_2$ for Euler-Bernoulli beam models can be found in (Elkaranshawy et al., 2018).

2.4. Dynamic Equilibrium Equation and The Time-Stepping Method

By applying Hamilton's principle, the dynamic equilibrium equation for ith beam element can be given as follows:

$$\mathbf{M}_i \ddot{\mathbf{q}}_i + \mathbf{C}_i \dot{\mathbf{q}}_i + \mathbf{F}_i^{int} - \mathbf{F}_i^{ext} = 0 \tag{2-28}$$

where $\mathbf{C}_i$, $\mathbf{F}_i^{ext}$, and $\ddot{\mathbf{q}}_i$ are the damping matrix, external load, and acceleration of the beam element in the global coordinate system, respectively. For the overall beam structure, equation (2-28) can be written as:

$$\mathbf{M}_i \ddot{\mathbf{q}}_i + \mathbf{C}_i \dot{\mathbf{q}}_i + \mathbf{F}_i^{int} - \mathbf{F}_i^{ext} = 0 \tag{2-29}$$

For the time-integration method, Newmark's implicit scheme is employed. In this scheme, at the next time step (n+1) the displacement and velocity of a node are expressed as follows:

$$\mathbf{q}_{n+1} = \mathbf{q}_n + dt\dot{\mathbf{q}}_n + \frac{dt^2}{2}[(1-2\chi)\ddot{\mathbf{q}}_n + 2\chi\ddot{\mathbf{q}}_{n+1}] \tag{2-30}$$

$$\dot{\mathbf{q}}_{n+1} = \dot{\mathbf{q}}_n + dt[(1-\gamma)\ddot{\mathbf{q}}_n + \gamma\ddot{\mathbf{q}}_{n+1}] \tag{2-31}$$

where *dt* is the time increment, and n is the current time step. In the present work, Newmark parameters are χ = 0.25 and γ = 0.5 to assure that the scheme is unconditionally stable.

A predictor-corrector procedure is implemented to solve the dynamic equilibrium in equation (2-27). In the predictor-step, the dynamic out of balance load can be expressed as:

$$\mathbf{R} = \mathbf{M}\left(\ddot{\mathbf{q}}_n + \frac{4}{dt}\dot{\mathbf{q}}_n\right) + \mathbf{C}\dot{\mathbf{q}}_n + \mathbf{F}_n^{int} - \mathbf{F}_n^{ext} \tag{2-32}$$

The displacement increment at n+1 is then predicted as:

$$d\mathbf{q}_{n+1}^p = -\mathbf{K}_{dyn}^{-1}\mathbf{R} \tag{2-33}$$

where the dynamic stiffness matrix $\mathbf{K}_{dyn}\mathbf{K}_{dyn}$ is defined by:

$$\mathbf{K}_{dyn} = \mathbf{K} + \frac{4}{dt^2}\mathbf{M} + \frac{2}{dt}\mathbf{C} \tag{2-34}$$

Hence, the predicted displacement, velocity, and acceleration vectors of each node are taking the following forms:

$$\mathbf{q}_{n+1}^p = \mathbf{q}_n + d\mathbf{q}_{n+1}^p \tag{2-35}$$

$$\dot{\mathbf{q}}_{n+1}^p = \dot{\mathbf{q}}_n + \frac{2}{dt}d\mathbf{q}_{n+1}^p \tag{2-36}$$

$$\ddot{\mathbf{q}}_{n+1}^p = \ddot{\mathbf{q}}_n + \frac{4}{dt^2}d\mathbf{q}_{n+1}^p \tag{2-37}$$

The variables obtained at the predictor step are corrected iteratively. In the corrector step, the dynamic out of balance load is expressed as:

$$\mathbf{R} = \mathbf{M}\ddot{\mathbf{q}}^{p}_{n+1} + \mathbf{C}\dot{\mathbf{q}}^{p}_{n+1} + \mathbf{F}^{int}_{n} - \mathbf{F}^{ext}_{n} \tag{2-38}$$

The displacement increment at n+1 is then corrected as:

$$d\mathbf{q}^{c}_{n+1} = -\mathbf{K}^{-1}_{dyn}\mathbf{R} \tag{2-39}$$

Thus, the displacement, velocity, and acceleration vectors of each node are corrected as:

$$\mathbf{q}^{c}_{n+1} = \mathbf{q}^{p}_{n+1} + d\mathbf{q}^{c}_{n+1} \tag{2-40}$$

$$\dot{\mathbf{q}}^{c}_{n+1} = \dot{\mathbf{q}}^{p}_{n+1} + \frac{2}{dt}d\mathbf{q}^{c}_{n+1} \tag{2-41}$$

$$\ddot{\mathbf{q}}^{c}_{n+1} = \ddot{\mathbf{q}}^{p}_{n+1} + \frac{4}{dt^{2}}d\mathbf{q}^{c}_{n+1} \tag{2-42}$$

At the corrector-step iteration, the values of predicted variables in equations (2-37) and (2-40) – (2-42) are simply replaced by the corrected values obtained at the current step. The details of this predictor-corrector procedure of Newmark's implicit method can be found in (Crisfield, 1997).

Regarding the convergence criterion, the energy-convergent criterion is used. Here, the dynamic equilibrium stage is obtained if:

$$\Phi^{(n)} \leq e_r . \Phi^{(n)} \tag{2-43}$$

where Φ is the residual energy, defined by

$$\Phi = \left\| \mathbf{R}^{T} . d\mathbf{q} \right\| \tag{2-44}$$

and $d\mathbf{q}$ is the residual displacement.

2.5. Numerical Algorithm

After initializing all variables such as beam geometry, beam mechanical properties, and load data, the algorithm for dynamic analysis of the 2D corotational beam formulation proceeds as follows:

1) Define the time step (dt) and the number of time steps (n_t). The final time (tf) is defined as $t_f = n_t.dt$
2) Start loop for n = 0 to n = n_t -1
   a) Determine the current global external load vector
   a) Calculate $\mathbf{k_i k_i}$, $\mathbf{m_i m_i}$, and $\mathbf{f_i^{int} f_i^{int}}$ for each element using equations (2-17), (2-27), and (2-24), respectively. It should be noted that these calculations use the current equilibrium configuration values ($\bar{\mathbf{q}}_i\bar{\mathbf{q}}_i$).
   b) Compute $\mathbf{K_i K_i}$, $\mathbf{M_i}$ $\mathbf{M_i}$, and $\mathbf{F_i^{int} F_i^{int}}$ for each element using equations (2-22), (2-26), and (2-23), respectively.
   c) Assembly the **KK**, **MM**, and $\mathbf{F^{int} F^{int}}$ of the overall structure.
   d) Compute the residual load vector and the residual displacement vector using equations (2-32) and (2-33), respectively.
   e) Calculate the residual energy using equation (2-44). If the residual energy satisfies the condition of the convergence criterion in equation (2-43), go to step (2-i).
   f) Otherwise, perform the predictor step to obtain initial vectors of the displacement, velocity, and acceleration of each node using equations (2-35) - (2-37).
   g) Perform the corrector step. Start iteration for k = 0 to k = maximum iteration number
      1) Modify $\mathbf{k_i k_i}$, $\mathbf{m_i}$, and $\mathbf{f_i^{int}}$ for each element using equations (2-17), (2-27), and (2-24), respectively. It should be noted that these calculations are based on $\mathbf{q}^{c}_{n+1}\mathbf{q}^{c}_{n+1}$. It the first iteration $\mathbf{q}^{c}_{n+1} = \mathbf{q}^{p}_{n+1}$.
      2) Compute $\mathbf{K_i}$, $\mathbf{M_i}$, and $\mathbf{F_i^{int}}$ for each element using equations (2-22), (2-26), and (2-23), respectively.
      3) Assembly the **K**, **M**, and $\mathbf{F^{int}}$ of the overall structure.
      4) Calculate the residual load vector and the residual displacement vector using

equations (2-38) and (2-39), respectively.

5) Compute the corrected displacement, velocity, and acceleration of each node using equations (2-40) – (2-42).
6) Calculate the residual energy using equation (2-44). If the residual energy satisfies the condition of the convergence criterion in equation (2-43), stop iteration and go to step (2-i).
7) Otherwise, extract $\mathbf{q}_i$, $\dot{\mathbf{q}}_i$, and $\ddot{\mathbf{q}}_i$.
8) Update $\bar{\mathbf{q}}_i$ for each element using equations (2-3) - (2-6).
9) Go to step (2-h-1) again to start a new iteration.

h) Update $\mathbf{q}_{n+1} = \mathbf{q}^c_{n+1}$, $\dot{\mathbf{q}}_{n+1} = \dot{\mathbf{q}}^c_{n+1}$, and $\ddot{\mathbf{q}}_{n+1} = \ddot{\mathbf{q}}^c_{n+1}$.
i) Extract $\mathbf{q}_i$ from $\mathbf{q}_{n+1}$.
j) Update $\bar{\mathbf{q}}_i$ for each element using equations (2-3) - (2-6).
k) Go to step (2-a) to start the next time step calculation.

3. Result and Analysis

In this section, four numerical examples are simulated and compared with the results found in the literature to investigate the accuracy and efficiency of the implemented algorithm and formulation. The structural damping is neglected. The tolerance error in all numerical tests is 10^{-12}, a very small parameter to demonstrate the efficiency and stability of proposed formulation.

3.1. Fixed-Fixed Beam under A Concentrated Vertical Load at Midspan

In this example, a constant point load of P = 640 lb is applied at the midspan of a fixed-fixed end beam as depicted in Figure 3-1. The beam has a length (L) of 20 in and a rectangular cross-section with a width (b) of 1 in and thickness (h) of 0.125 in. The Young's modulus is E = 3.10^6 Psi, the Poisson's ratio is ν = 0, and the material density is ρ = 2.536 x 10^{-4} s^2/in^4. No damping is considered and the beam is discretized using 20 uniform elements.

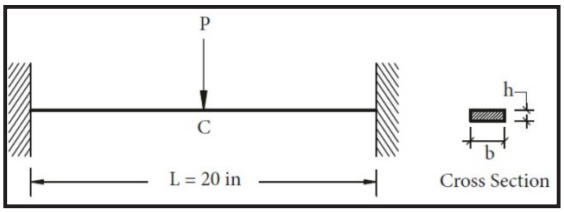

Figure 3-1: Fixed-fixed beam under a concentrated load at midspan (Elkaranshawy et al., 2018).

This problem was solved by Elkaranshawy et al. (2018) using a 2D corotational method, the same method as used in the proposed formulation. However, both formulations are different in terms of the internal elastic force calculation and the convergence criterion. In addition, they used a very small time step size (dt) of 5.10^{-5} s, whereas the present simulation only uses dt = 10^{-2} s. The simulation is carried out up to 5 ms and the result is compared with that reported in (Elkaranshawy et al., 2018). As shown in Figure 3-2, the present study confirmed the results obtained in (Elkaranshawy et al., 2018). The important point of this result is that the proposed algorithm is more efficient than that used in (Elkaranshawy et al., 2018) since the time step size used in the present simulation is much larger than that used in (Elkaranshawy et al., 2018).

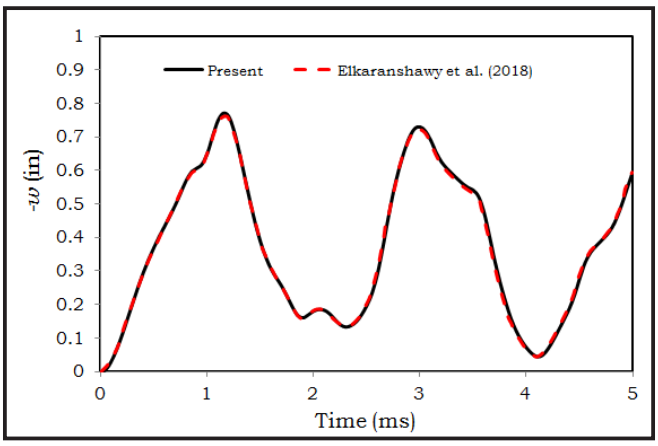

Figure 3-2: Vertical displacement at midspan of a fixed-fixed beam due to a constant vertical load.

3.2. Cantilever Beam Under A Sinusoidal Point Load

In this example, a sinusoidal vertical load of $P = P_0.\sin(\omega t)$ is applied at the tip of a cantilever beam as shown in Figure 3-3. The beam has a length (L) of 10 m and a rectangular cross-section with a width (b) of 0.5 m and thickness (h) of 0.25. The Young's modulus is E = 210 GPa, the Poisson's ratio is ν = 0.3 and the material density is ρ = 7850 kg/m. No damping is considered and the beam is discretized using 10 uniform elements. Constant time step size dt = 10^{-4} s is used and the simulation is carried out up to 1.5 s.

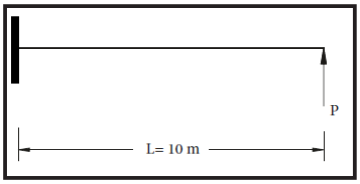

Figure 3-3: Cantilever beam subjected to a tip load

This problem was solved by Le et al. (2011) using corotational formulation and a result obtained from Total Lagrangian Formulation with 48 elements was used as the reference solution (Le et al., 2011). Elkaranshawy et al. (2018) also analyzed the same problem using 2D corotational formulation. The results of the present simulation are identical to those reported in (Elkaranshawy et al., 2018). Hence, the results are only compared with those reported in (Le et al., 2011), as given in Figure 3-4. By considering the excellent agreement between the present results and the reference solution used in (Le et al., 2011), it can be said that the results of the proposed algorithm are more accurate than those obtained by Le et al. (Le et al., 2011).

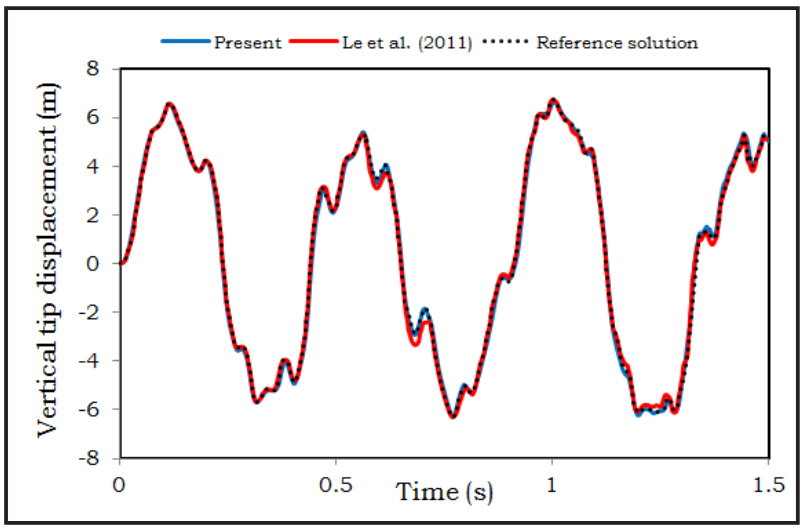

Figure 3-4: Tip vertical displacement of a cantilever beam due to a sinusoidal point load

3.3. Flying Flexible Beam

This problem was first introduced by Simo & Vu-Quoc (1988) to analyze the dynamics of rods in space and later studied also in (Hsiao et al., 1999; Marino et al., 2019; Zhang & Zhong, 2016; Zupan et al., 2012) for the 3D case and in (Chróścielewski et al., 2000; Elkaranshawy & Dokainish, 1995) for the 2D case. In the 2D simulation, an initially inclined straight flexible beam without kinematic constraints is loaded by time-varying force P and torque M at the lower end of the beam as depicted in Figure 3-5. The geometry of the initial configuration, the material properties of the beam, and the time history of these loads are also shown in that figure. Due to the absence of kinematic constraints, the linear and angular momenta as well as the potential and kinetic energy of the beam must be conserved after fully unloading. This makes this problem a perfect numerical example to test the energy-momentum preserving properties of the proposed formulation. This problem also produces a complex dynamic behavior characterized by a forward translational motion due to P, and a forward tumbling due to M (Marino et al., 2019).

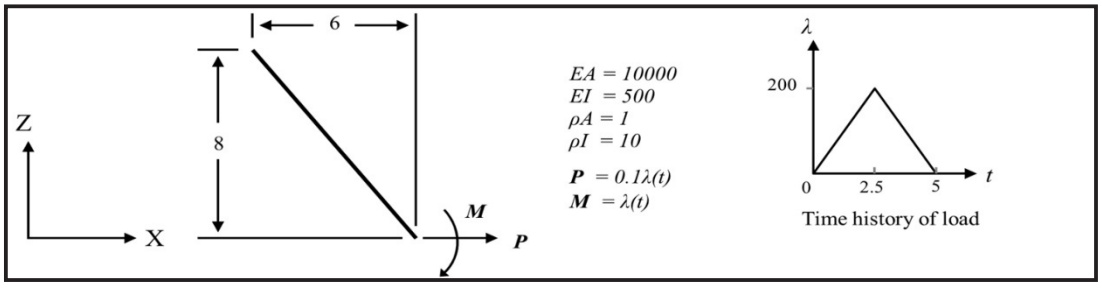

Figure 3-5: Geometric, material, and loading data of flying flexible beam.

The beam is modeled by 20 elements and the simulation is performed for t = 10 using constant time step sizes dt = 0.01. In Figure 3-6, the deformation history of the beam is shown. The snapshots are taken at the same time instants as in (Chróścielewski et al., 2000) to ease the comparison. The results are in good agreement with those reported in (Chróścielewski et al., 2000). The total energy history plot from time 0 to 500 is given in Figure 3-7. This also confirms the data presented by (Chróścielewski et al., 2000).It can be said that the results confirm the dynamical behavior of the flying flexible beam as also discussed in (Chróścielewski et al., 2000; Elkaranshawy & Dokainish, 1995; Hsiao et al., 1999; Marino et al., 2019; Zhang & Zhong, 2016; Zupan et al., 2012).

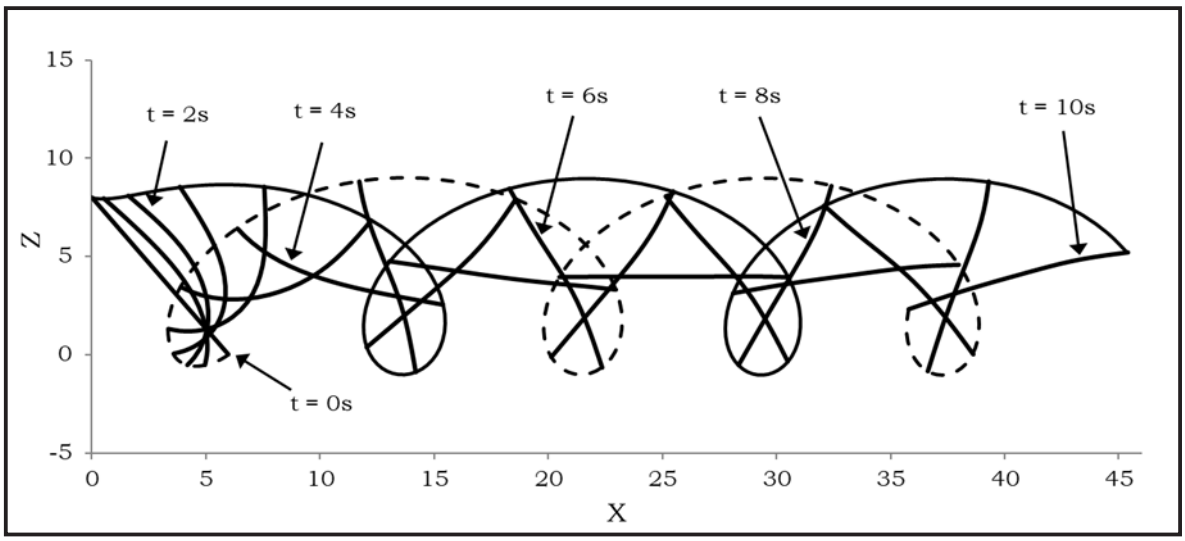

Figure 3-6: Snapshots of the tumbling history of flying flexible flying beam in 2D motion.

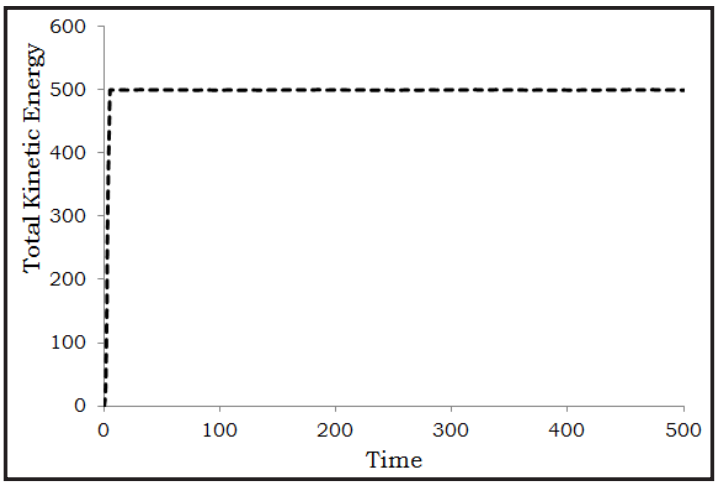

Figure 3-7: Time history of the total energy of flying flexible beam.

Considering the large time step size and the number of time steps applied in the simulation, the present results show that the proposed method is efficient and capable of simulating a long-time dynamic analysis. This claim is supported by the result which indicates that the total energy of the system is constant in the absence of external loads even if a very large number of time steps is used. Conserving the energy and momentum is crucial for performing long-time dynamic analysis such as in Fluid-Structure Interaction (FSI) simulations. Hence, it can be said that the proposed formulation can be used to study 2D FSI problems. However, it should be mentioned that the proposed algorithm is not intended to have this energy-momentum preserving property. The application of energy-convergent criterion does not mean that the energy-momentum conserving algorithm is implemented in the proposed algorithm.

3.4. Swinging of A Rubber-Like Beam

A simulation of the free falling of a flexible beam under gravity is presented to validate the accuracy and capability of the present structural solver in predicting the large-displacement responses. An initially horizontal flexible beam is hinged at its root and free at its tip. The beam swings due to the gravity effect once it is released. The beam is very flexible, intended to produce extremely large displacement. The beam has a length of 1.0 m and a circular cross-section with a diameter of 0.01 m. The Young's modulus is E = 5×106 Pa, the Poisson's ratio is $\nu\nu$ = 0.5 and the material density is $\rho\rho$ = 1100 kg/m. The beam is only loaded by its self-weight with g = 9.81 m/s^2. No damping is considered and the beam is discretized using 20 elements. The simulation is performed for 1s using constant time step sizes dt = 0.01 s. The

snapshots of the swinging flexible beam are presented in Figure 3-8.

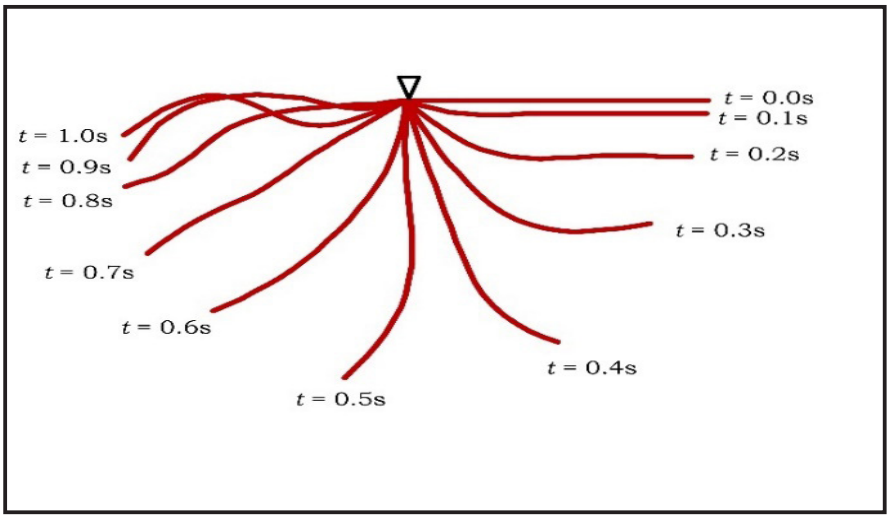

Figure 3-8: Snapshots of a swinging flexible beam taken from time 0 to 1s with increments of 0.1s

The time history of the vertical tip displacement is compared with the results obtained from (Lang et al., 2011; Marino et al., 2019; Weeger et al., 2017) as shown in Figure 3-9. Marino et al. (2019) and Weeger et al. (2017) solved this problem using an iso-geometric collocation method, whilst Lang et al. (2011) used the Cosserat's geometrically exact theory of rods. The figure shows that the present simulation result is in excellent agreement with the published works.

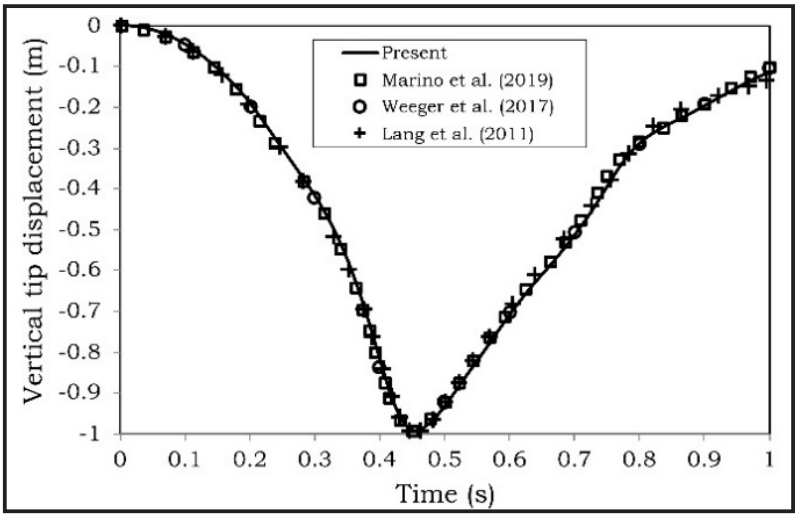

Figure 3-9: Comparison of vertical tip displacement of a swinging flexible beam with the published literature

4. Conclusions

In this paper, a simple and efficient corotational dynamic formulation for geometrically nonlinear of 2D flexible beams is presented. Local formulation of the beam element employs the classical Hermitian shape functions. The proposed formulation implements a simple geometric stiffness matrix and can efficiently define the internal load vector. The nonlinear dynamic equilibrium equation is solved iteratively by Newmark's implicit time-integration scheme with the predictor-corrector algorithm.

Four numerical examples of flexible beams undergoing large deformation are simulated in the present work. The results of the proposed formulation are compared with the reference data found in the literature. In all examples, an excellent agreement is obtained between the

present simulation results and the reference data. Accurate results with great efficiency are still achieved, even though simulations only used a small number of elements. The study concludes that the results obtained in the present study confirm the reliability, accuracy, and efficiency of the proposed 2D corotational beam formulation.

Acknowledgements

The first author would like to greatly acknowledge the Indonesia Endowment Fund for Education (LPDP), Ministry of Finance of the Republic of Indonesia, for the support granted on this research at Institut Teknologi Bandung.

Contributorship Statement

NA designed method, developed the simulation, and prepared the manuscript; LRZ supervised the simulation and the manuscript writing; HM and LG verified the simulation results. All authors discussed the results and contributed to the final manuscript.

References

Alsafadie, R., Hjiaj, M., & Battini, J. M. (2011). Three-dimensional formulation of a mixed corotational thin-walled beam element incorporating shear and warping deformation. *Thin-Walled Structures*, *49*(4), 523–533. https://doi.org/10.1016/j.tws.2010.12.002

Andria, N., Zuhal, L. R., Gunawan, L., & Muhammad, H. (2019). Metoda corotational beam 2D untuk analisis statik struktur nonlinier geometrik (A 2D corotational beam method for geometrically nonlinear static structural analysis). *Jurnal Teknologi Dirgantara*, *17*(1), 79–90.

Behdinan, K., Stylianou, M. C., & Tabarrok, B. (1998). Co-rotational dynamic analysis of flexible beams. *Computer Methods in Applied Mechanics and Engineering*, *154*(3–4), 151–161. https://doi.org/10.1016/S0045-7825(97)00124-2

Chróścielewski, J., Makowski, J., & Pietraszkiewicz, W. (2000). Large Overall Motion of Flexible Branched Shell Structures. *Computational Aspects of Nonlinear Structural Systems with Large Rigid Body Motion. NATO Advanced Research Workshop*, *3*, 201–218.

Crisfield, M. A. (1997). *Non-Linear Finite Element Analysis of Solids and Structures, Volume 2: Advanced Topics*. John Wiley & Sons Ltd,.

Crisfield, M. A., & Cole, G. (1990). Co-rotational beam elements for two- and three-dimensional structures. *Discretisation Methods in Structural Mechanics*, 1–2.

Durand, R., Pantoja-Rosero, B. G., & Oliveira, V. (2019). A general mesh smoothing method for finite elements. *Finite Elements in Analysis and Design*, *158*, 17–30. https://doi.org/10.1016/J.FINEL.2019.01.010

Elkaranshawy, H. A., & Dokainish, M. A. (1995). Corotational finite element analysis of planar flexible multibody systems. *Computers and Structures*, *54*(5), 881–890. https://doi.org/10.1016/0045-7949(94)00346-5

Elkaranshawy, H. A., Elerian, A. A. H., & Hussien, W. I. (2018). A Corotational Formulation Based on Hamilton's Principle for Geometrically Nonlinear Thin and Thick Planar Beams and Frames. *Mathematical Problems in Engineering*, *2018*. https://doi.org/10.1155/2018/2670462

Hsiao, K. M., Lin, J. Y., & Lin, W. Y. (1999). A consistent co-rotational finite element formulation for geometrically nonlinear dynamic analysis of 3-D beams. *Computer Methods in Applied Mechanics and Engineering*, *169*(1–2), 1–18. https://doi.org/10.1016/S0045-7825(98)00152-2

Kan, Z., Dong, K., Chen, B., Peng, H., & Song, X. (2021). The direct force correction based framework for general co-rotational analysis. *Computer Methods in Applied Mechanics*

and Engineering, *385*, 114018. https://doi.org/10.1016/j.cma.2021.114018

Lang, H., Linn, J., & Arnold, M. (2011). Multi-body dynamics simulation of geometrically exact Cosserat rods. *Multibody System Dynamics*, *25*(3), 285–312. https://doi.org/10.1007/s11044-010-9223-x

Le, T. N., Battini, J. M., & Hjiaj, M. (2011). Efficient formulation for dynamics of corotational 2D beams. *Computational Mechanics*, *48*(2), 153–161. https://doi.org/10.1007/s00466-011-0585-6

Le, T. N., Battini, J. M., & Hjiaj, M. (2012). Dynamics of 3D beam elements in a corotational context: A comparative study of established and new formulations. *Finite Elements in Analysis and Design*, *61*, 97–111. https://doi.org/10.1016/j.finel.2012.06.007

Le, T. N., Battini, J. M., & Hjiaj, M. (2014a). A consistent 3D corotational beam element for nonlinear dynamic analysis of flexible structures. *Computer Methods in Applied Mechanics and Engineering*, *269*, 538–565. https://doi.org/10.1016/j.cma.2013.11.007

Le, T. N., Battini, J. M., & Hjiaj, M. (2014b). Corotational formulation for nonlinear dynamics of beams with arbitrary thin-walled open cross-sections. *Computers and Structures*, *134*, 112–127. https://doi.org/10.1016/j.compstruc.2013.11.005

Levyakov, S. V. (2015). Formulation of a geometrically nonlinear 3D beam finite element based on kinematic-group approach. *Applied Mathematical Modelling*, *39*(20), 6207–6222. https://doi.org/10.1016/j.apm.2015.01.064

Luo, Y. (2008). Dealing with extremely large deformation by Nearest-Nodes FEM with algorithm for updating element connectivity. *International Journal of Solids and Structures*, *45*(18–19), 5074–5087. https://doi.org/10.1016/J.IJSOLSTR.2008.05.006

Ma, Z., Liu, Z., & You, P. (2023). A 3D corotational beam element formulated on the special Euclidean group SE(3). *Computers & Structures*, *281*, 107011. https://doi.org/10.1016/j.compstruc.2023.107011

Marino, E., Kiendl, J., & De Lorenzis, L. (2019). Explicit isogeometric collocation for the dynamics of three-dimensional beams undergoing finite motions. *Computer Methods in Applied Mechanics and Engineering*, *343*, 530–549. https://doi.org/10.1016/j.cma.2018.09.005

Simo, J. C., & Vu-Quoc, L. (1988). On the dynamics in space of rods undergoing large motions—A geometrically exact approach. *Computer Methods in Applied Mechanics and Engineering*, *66*(2), 125–161. https://doi.org/10.1016/0045-7825(88)90073-4

Wang, D., Randolph, M. F., & White, D. J. (2013). A dynamic large deformation finite element method based on mesh regeneration. *Computers and Geotechnics*, *54*, 192–201. https://doi.org/10.1016/J.COMPGEO.2013.07.005

Weeger, O., Narayanan, B., De Lorenzis, L., Kiendl, J., & Dunn, M. L. (2017). An isogeometric collocation method for frictionless contact of Cosserat rods. *Computer Methods in Applied Mechanics and Engineering*, *321*, 361–382. https://doi.org/10.1016/j.cma.2017.04.014

You, P., Liu, Z., & Ma, Z. (2024). A contact formulation using local frame of SE(3) group for corotational beam against rigid solid via moving signed distance field. *Computer Methods in Applied Mechanics and Engineering*, *418*, 116532. https://doi.org/10.1016/j.cma.2023.116532

Zhang, R., & Zhong, H. (2016). A quadrature element formulation of an energy–momentum conserving algorithm for dynamic analysis of geometrically exact beams. *Computers & Structures*, *165*, 96–106. https://doi.org/10.1016/J.COMPSTRUC.2015.12.007

Zupan, E., Saje, M., & Zupan, D. (2012). Quaternion-based dynamics of geometrically non-linear spatial beams using the RungeKutta method. *Finite Elements in Analysis and Design*, *54*, 48–60. https://doi.org/10.1016/j.finel.2012.01.007